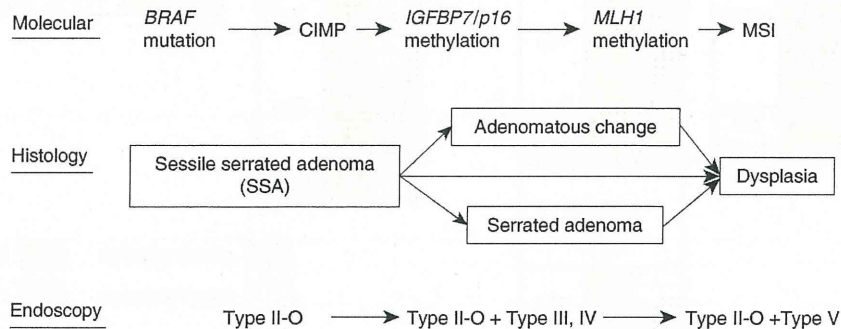


**Figure 4.** Clinical usefulness of the Type II open-shape (Type II-O) pit pattern for defining sessile serrated adenomas (SSAs). (a) A diagnostic tree to identify SSAs with *BRAF* mutation and CpG island methylator phenotype (CIMP). Serrated lesions are classified into four groups according to their pit patterns. The ratios of *BRAF*-mutant plus CIMP-positive lesions in the respective groups of the training and validation sets are shown below. (b) Receiver operating characteristic (ROC) curve analysis of the performance of the diagnostic tree. Sensitivities and specificities for definition of *BRAF*-mutant plus CIMP-positive lesions were calculated at three cutoffs for each group (group 1 vs. groups 2–4; groups 1–2 vs. groups 3–4; groups 1–3 vs. group 4).



**Figure 5.** Progression of the molecular, histological and colonoscopic features in the serrated neoplastic pathway.

target of p53 (27,30). In CRCs, methylation of *IGFBP7* is strongly associated with *BRAF* mutation, the lack of p53 mutation and the presence of MSI and CIMP (27). In the present study, we showed

that levels of *IGFBP7* methylation are elevated in Type II-O pit-positive serrated lesions, suggesting the tumor suppressor function of p53 is attenuated at an early stage of the MSI pathway.

The mechanism underlying the strong relationship between Type II-O pits and SSAs remains unclear. SSAs exhibit a variety of histological features, including exaggerated serration, boot-shaped crypts, and the branching and dilatation of the crypts (8,15,31). These features are usually observed near the base of the crypts, making it difficult to endoscopically discriminate SSAs from HPs. SSAs are often covered by abundant mucus production, and accumulation of the mucin within crypts may lead to their dilatation (31). It is thus conceivable that overproduction of mucin may be associated with the Type II-O pit pattern in SSAs.

Identification of SSAs in screening colonoscopies has great significance for the prevention and surveillance of CRCs, as it is generally accepted that colonoscopy and polypectomy reduce the incidence of CRCs (32–35). Although SSAs are usually treated as conventional adenomas, it is still uncertain whether all SSAs should be endoscopically resected (16,36). In the present study, a large majority of Type II-O-positive lesions were histologically SSAs, and were tightly associated with *BRAF* mutation and CIMP, suggesting these lesions are appropriate targets for endoscopic resection. Moreover, as serrated lesions with Type II-O plus Type III, IV or V pits exhibit additional malignant potential, they too should be targets of early treatment. On the other hand, we noted that approximately half of the serrated lesions with only conventional Type II pits in our validation set were diagnosed as SSAs, though all Type II lesions in the training set were HP/IMs. This difference reflects the extremely high specificity and relatively low sensitivity of Type II-O pits for distinguishing SSAs from HP/IMs (Table 1).

There are several possible explanations for the low sensitivity of Type II-O pits for definition of SSAs. First, SSAs with only conventional Type II pits in our validation set may have been at a very early stage of development, where Type II-O pits were not yet established. Alternatively, it may simply reflect the difficulty of histologically distinguishing SSAs from HP/IMs. Of these two possibilities, the first is supported by the fact that although *BRAF* was frequently mutated in these lesions, aberrant DNA methylation was infrequent and only a limited number of the specimens were CIMP-positive. Further prospective study will be needed to unravel the time course of the emergence of Type II-O pits in the serrated pathway.

There are several potential limitations to the current study. First, our diagnostic system is based on endoscopic observations, so it may be affected by the skills of the endoscopists. As described above, among the ten endoscopists participating in this study, four had experience with more than 1,000 endoscopy cases, whereas the remaining six were less experienced. We therefore divided the data into two parts according to the endoscopists' experience and compared the diagnostic accuracy of Type II-O pits for defining SSAs. As shown in **Supplementary Table 4**, the sensitivities and specificities were similar between the two groups, suggesting the intra-observer variability in our diagnostic system is relatively limited. Second, there are several biases in the selection of tumor specimens in this study. For instance, the average size of the lesions is relatively large

(>10 mm). This is because these specimens were collected through endoscopic resection, and smaller lesions, which are usually subject to follow-up observation, were less likely to be included in this study. In addition, during the collection of the training set specimens, we treated as many possible serrated lesions as possible, which might have resulted in a somewhat high frequency of TSAs in our training set. Moreover, the identification of Type II-O pits enabled us to distinguish non-neoplastic HP/IM from neoplastic serrated lesions, which might have reduced the frequency of HP/IM in the validation set. Thus, our findings should be validated in an independent multicenter study that includes a larger number of samples. Third, our study does not provide effective criteria to endoscopically define TSAs. Further study may enable us to find new clues to refine the endoscopic diagnosis of serrated lesions.

In summary, we have identified a novel surface microstructure that is specific to SSAs. Recent studies have shown that the presence of SSAs is associated with an increased risk of synchronous CRCs (37–40). In the context of those findings, our observations indicate detection of Type II-O pits could be predictive of CRC risk. Thus, more intensive and frequent colonoscopic surveillance may be appropriate for patients in whom Type II-O-positive lesions were once detected. Not only could these findings contribute to the prevention of MSI-positive CRCs, they also demonstrate that integrative analysis of molecular and endoscopic characteristics greatly improves our understanding of the pathogenesis of CRC and the quality of colonoscopic surveillance.

#### ACKNOWLEDGMENT

The authors thank Dr William F. Goldman for editing the manuscript.

#### CONFLICT OF INTEREST

**Guarantor of the article:** Hiromu Suzuki, MD, PhD.

**Specific author contributions:** T. Kimura, E. Yamamoto, H. Yamano and M. Toyota conceived the study; E. Yamamoto, H. Suzuki, K. Imai, Y. Shinomura and M. Toyota designed the study; E. Yamamoto and H. Suzuki wrote the manuscript; T. Kimura, H. Yamano, K. Yoshikawa, R. Takagi, R. Kato, T. Harada and R. Suzuki carried out material support; T. Sugai performed histological analysis; M. Nojima performed statistical analysis; S. Kamimae, T. Sawada, M. Ashida, R. Maruyama, M. Kai and T. Sugai carried out the experiments; E. Yamamoto, H. Suzuki, M. Nojima performed data analysis.

**Financial support:** This study was supported in part by Grants-in-Aid for Scientific Research in Priority Areas (M. Toyota and K. Imai), a Grant-in-Aid for the Third-term Comprehensive 10-year Strategy for Cancer Control (M. Toyota), a Grant-in-Aid for Cancer Research from the Ministry of Health, Labor and Welfare, Japan (M. Toyota), and a Research Grant from the Princess Takamatsu Cancer Research Fund 09-24119 (M. Toyota).

**Potential competing interest:** None.



## Study Highlights

### WHAT IS CURRENT KNOWLEDGE

- ✓ Recent evidence suggests that sessile serrated adenomas (SSAs) are precursor lesions for colorectal cancers (CRCs) with microsatellite instability (MSI).
- ✓ Pit pattern analysis using magnifying colonoscopy is an effective method of distinguishing malignant from benign lesions.

### WHAT IS NEW HERE

- ✓ The Type II open-shape pit pattern (Type II-O) is a novel surface microstructure specific to SSAs.
- ✓ The presence of the Type II-O pit pattern is a hallmark of the premalignant stage of MSI and CpG island methylator phenotype (CIMP)-positive CRCs.
- ✓ Our findings will improve the efficacy of colonoscopic surveillance to prevent CRCs, especially those with MSI and CIMP.

### REFERENCES

1. Vogelstein B, Fearon ER, Hamilton SR *et al*. Genetic alterations during colorectal-tumor development. *N Engl J Med* 1988;319:525–32.
2. Jones PA, Baylin SB. The epigenomics of cancer. *Cell* 2007;128:683–92.
3. Toyota M, Ahuja N, Ohe-Toyota M *et al*. CpG island methylator phenotype in colorectal cancer. *Proc Natl Acad Sci USA* 1999;96:8681–6.
4. Toyota M, Ohe-Toyota M, Ahuja N *et al*. Distinct genetic profiles in colorectal tumors with or without the CpG island methylator phenotype. *Proc Natl Acad Sci USA* 2000;97:710–5.
5. Weisenberger D, Siegmund K, Campan M *et al*. CpG island methylator phenotype underlies sporadic microsatellite instability and is tightly associated with BRAF mutation in colorectal cancer. *Nat Genet* 2006;38:787.
6. Shen L, Toyota M, Kondo Y *et al*. Integrated genetic and epigenetic analysis identifies three different subclasses of colon cancer. *Proc Natl Acad Sci USA* 2007;104:18654.
7. Longacre TA, Fenoglio-Preiser CM. Mixed hyperplastic adenomatous polyps/serrated adenomas. A distinct form of colorectal neoplasia. *Am J Surg Pathol* 1990;14:524–37.
8. Torlakovic E, Skovlund E, Snover D *et al*. Morphologic reappraisal of serrated colorectal polyps. *Am J Surg Pathol* 2003;27:65–81.
9. Snover D, Jass J, Fenoglio-Preiser C *et al*. Serrated polyps of the large intestine: a morphologic and molecular review of an evolving concept. *Am J Clin Pathol* 2005;124:380–91.
10. Farris A, Misraji J, Srivastava A *et al*. Sessile serrated adenoma: challenging discrimination from other serrated colonic polyps. *Am J Surg Pathol* 2008;32:30–5.
11. Torlakovic E, Gomez J, Driman D *et al*. Sessile serrated adenoma (SSA) vs. traditional serrated adenoma (TSA). *Am J Surg Pathol* 2008;32:21–9.
12. Hetzel J, Huang C, Coukos J *et al*. Variation in the detection of serrated polyps in an average risk colorectal cancer screening cohort. *Am J Gastroenterol* 2010;105:2656–64.
13. Kambara T, Simms LA, Whitehall VL *et al*. BRAF mutation is associated with DNA methylation in serrated polyps and cancers of the colorectum. *Gut* 2004;53:1137–44.
14. Spring KJ, Zhao ZZ, Karamatic R *et al*. High prevalence of sessile serrated adenomas with BRAF mutations: a prospective study of patients undergoing colonoscopy. *Gastroenterology* 2006;131:1400–7.
15. Jass JR, Baker K, Zlobec I *et al*. Advanced colorectal polyps with the molecular and morphological features of serrated polyps and adenomas: concept of a 'fusion' pathway to colorectal cancer. *Histopathology* 2006;49:121–31.
16. Leggett B, Whitehall V. Role of the serrated pathway in colorectal cancer pathogenesis. *Gastroenterology* 2010;138:2088–100.
17. Boparai KS, van den Broek FJ, van Eeden S *et al*. Hyperplastic polyposis syndrome: a pilot study for the differentiation of polyps by using high-resolution endoscopy, autofluorescence imaging, and narrow-band imaging. *Gastrointest Endosc* 2009;70:947–55.
18. Kudo S, Tamura S, Nakajima T *et al*. Diagnosis of colorectal tumorous lesions by magnifying endoscopy. *Gastrointest Endosc* 1996;44:8–14.
19. Hurlstone DP, Cross SS, Adam I *et al*. Efficacy of high magnification chromoscopic colonoscopy for the diagnosis of neoplasia in flat and depressed lesions of the colorectum: a prospective analysis. *Gut* 2004;53:284–90.
20. Kudo S, Lambert R, Allen J *et al*. Nonpolypoid neoplastic lesions of the colorectal mucosa. *Gastrointest Endosc* 2008;68:S3–47.
21. Matsuda T, Fujii T, Saito Y *et al*. Efficacy of the invasive/non-invasive pattern by magnifying chromoendoscopy to estimate the depth of invasion of early colorectal neoplasms. *Am J Gastroenterol* 2008;103:2700–6.
22. Morita T, Tamura S, Miyazaki J *et al*. Evaluation of endoscopic and histopathological features of serrated adenoma of the colon. *Endoscopy* 2001;33:761–5.
23. Oka S, Tanaka S, Hiyama T *et al*. Clinicopathologic and endoscopic features of colorectal serrated adenoma: differences between polypoid and superficial types. *Gastrointest Endosc* 2004;59:213–9.
24. Toyota M, Suzuki H, Sasaki Y *et al*. Epigenetic silencing of microRNA-34b/c and B-cell translocation gene 4 is associated with CpG island methylation in colorectal cancer. *Cancer Res* 2008;68:4123–32.
25. Sugai T, Habano W, Endoh M *et al*. Molecular analysis of gastric differentiated-type intramucosal and submucosal cancers. *Int J Cancer* 2010;127:2500–9.
26. Boland CR, Thibodeau SN, Hamilton SR *et al*. A National Cancer Institute Workshop on Microsatellite Instability for cancer detection and familial predisposition: development of international criteria for the determination of microsatellite instability in colorectal cancer. *Cancer Res* 1998;58:5248–57.
27. Suzuki H, Igarashi S, Nojima M *et al*. IGFBP7 is a p53-responsive gene specifically silenced in colorectal cancer with CpG island methylator phenotype. *Carcinogenesis* 2010;31:342–9.
28. Serrano M, Lin AW, McCurrach ME *et al*. Oncogenic ras provokes premature cell senescence associated with accumulation of p53 and p16INK4a. *Cell* 1997;88:593–602.
29. Collado M, Serrano M. The power and the promise of oncogene-induced senescence markers. *Nat Rev Cancer* 2006;6:472–6.
30. Wajapeyee N, Serra RW, Zhu X *et al*. Oncogenic BRAF induces senescence and apoptosis through pathways mediated by the secreted protein IGFBP7. *Cell* 2008;132:363–74.
31. Higuchi T, Sugihara K, Jass JR. Demographic and pathological characteristics of serrated polyps of colorectum. *Histopathology* 2005;47:32–40.
32. Winawer SJ, Zauber AG, Ho MN *et al*. Prevention of colorectal cancer by colonoscopic polypectomy. The National Polyp Study Workgroup. *N Engl J Med* 1993;329:1977–81.
33. Citarda F, Tomaselli G, Capocaccia R *et al*. Efficacy in standard clinical practice of colonoscopic polypectomy in reducing colorectal cancer incidence. *Gut* 2001;48:812–5.
34. Brenner H, Chang-Claude J, Seiler CM *et al*. Does a negative screening colonoscopy ever need to be repeated? *Gut* 2006;55:1145–50.
35. Winawer S, Zauber A, Fletcher R *et al*. Guidelines for colonoscopy surveillance after polypectomy: a consensus update by the US Multi-Society Task Force on Colorectal Cancer and the American Cancer Society. *Gastroenterology* 2006;130:1872–85.
36. Jass J. Gastrointestinal polyposis: clinical, pathological and molecular features. *Gastroenterol Clin North Am* 2007;36:927–46, viii.
37. Li D, Jin C, McCulloch C *et al*. Association of large serrated polyps with synchronous advanced colorectal neoplasia. *Am J Gastroenterol* 2009;104:695.
38. Hiraoka S, Kato J, Fujiki S *et al*. The presence of large serrated polyps increases risk for colorectal cancer. *Gastroenterology* 2010;139: 1503,10, 1510.e1–3.
39. Schreiner MA, Weiss DG, Lieberman DA. Proximal and large hyperplastic and nondysplastic serrated polyps detected by colonoscopy are associated with neoplasia. *Gastroenterology* 2010;139:1497–502.
40. Boparai K, Mathus-Vliegen EMH, Koornstra J *et al*. Increased colorectal cancer risk during follow-up in patients with hyperplastic polyposis syndrome: a multicentre cohort study. *Gut* 2010;59:1094–100.



## Upregulation of miR-196a and *HOTAIR* Drive Malignant Character in Gastrointestinal Stromal Tumors

Takeshi Niinuma<sup>1</sup>, Hiromu Suzuki<sup>1,3</sup>, Masanori Nojima<sup>4</sup>, Katsuhiko Noshō<sup>1</sup>, Hiroyuki Yamamoto<sup>1</sup>, Hiroyuki Takamaru<sup>1</sup>, Eiichiro Yamamoto<sup>3</sup>, Reo Maruyama<sup>3</sup>, Takayuki Nobuoka<sup>2</sup>, Yasuaki Miyazaki<sup>9</sup>, Toshiro Nishida<sup>9,10</sup>, Takeo Bamba<sup>11</sup>, Tatsuo Kanda<sup>11</sup>, Yoichi Ajioka<sup>12</sup>, Takahiro Taguchi<sup>13</sup>, Satoshi Okahara<sup>7</sup>, Hiroaki Takahashi<sup>7</sup>, Yasunori Nishida<sup>8</sup>, Masao Hosokawa<sup>8</sup>, Tadashi Hasegawa<sup>5</sup>, Takashi Tokino<sup>6</sup>, Koichi Hirata<sup>2</sup>, Kohzoh Imai<sup>14</sup>, Minoru Toyota<sup>3</sup>, and Yasuhisa Shinomura<sup>1</sup>

### Abstract

Large intergenic noncoding RNAs (lincRNA) have been less studied than miRNAs in cancer, although both offer considerable therapeutic potential. In this study, we identified frequent upregulation of miR-196a and lincRNA *HOTAIR* in high-risk gastrointestinal stromal tumors (GIST). Overexpression of miR-196a was associated with high-risk grade, metastasis and poor survival among GIST specimens. miR-196a genes are located within the *HOX* gene clusters and microarray expression analysis revealed that the *HOXC* and *HOTAIR* gene were also coordinately upregulated in GISTs which overexpress miR-196a. In like manner, overexpression of *HOTAIR* was also strongly associated with high-risk grade and metastasis among GIST specimens. RNA interference-mediated knockdown of *HOTAIR* altered the expression of reported *HOTAIR* target genes and suppressed GIST cell invasiveness. These findings reveal concurrent overexpression of *HOX* genes with noncoding RNAs in human cancer in this setting, revealing miR-196a and *HOTAIR* as potentially useful biomarkers and therapeutic targets in malignant GISTs. *Cancer Res*; 72(5); 1126–36. ©2012 AACR.

### Introduction

Gastrointestinal stromal tumors (GIST) are the most common mesenchymal tumors of the gastrointestinal tract (1–3). GISTs arise predominantly in the stomach (60%) and small intestine (25%) but also occur in colon and rectum (5%), esophagus (2%), and other organs (3). Immunohistochemically, GISTs are positive for KIT and CD34 and are negative or

variably positive for other neural and smooth muscle cell markers. The expression of KIT and CD34 is a characteristic feature of the intestinal cells of Cajal (ICC), which are located in the intestinal wall and regulate gastrointestinal motility. GISTs are thus thought to originate from ICCs or ICC precursors. Activating *KIT* mutations have been identified in 80% to 90% of GISTs, and mutation of the platelet-derived growth factor receptor alpha gene (*PDGFRA*) is observed in approximately 5% of GISTs (1–3). In that context, imatinib mesylate (formerly STI571) was developed as a tyrosine kinase inhibitor and has been shown to inhibit the activities of BCR-ABL, KIT, and PDGFR. Imatinib mesylate is currently being used for the treatment of both chronic myeloid leukemia and metastatic GISTs.

Predicting the biologic potential of GISTs is often difficult, and considerable effort has been made to define the variables that could enable more accurate identification of tumors with malignant potential. In most classification systems, the key prognostic factors for estimating malignant potential are tumor size and mitotic rate, and to a more variable degree, the proliferation index or tumor site (4). Other potential and promising markers of GIST malignancy are molecular alterations. As mentioned, a large majority of GISTs exhibit activating *KIT* or *PDGFRA* mutations. By itself, however, mutation status does not fully explain the diverse biology of GISTs, and it is believed that additional molecular alterations are required for the progression of high-risk GISTs. For instance, expression of CD26 (encoded by *DPP4*) is strongly associated with poor survival among patients with gastric GISTs, suggesting its involvement in the malignant progression of the disease (5).

**Authors' Affiliations:** First Departments of <sup>1</sup>Internal Medicine and <sup>2</sup>Surgery, Departments of <sup>3</sup>Molecular Biology, <sup>4</sup>Public Health, <sup>5</sup>Surgical Pathology, <sup>6</sup>Medical Genome Science, Research Institute for Frontier Medicine, Sapporo Medical University School of Medicine; Departments of <sup>7</sup>Gastroenterology and <sup>8</sup>Surgery, Keiyukai Sapporo Hospital, Sapporo; <sup>9</sup>Department of Surgery, Osaka University Graduate School of Medicine; <sup>10</sup>Department of Surgery, Osaka Police Hospital, Osaka; Divisions of <sup>11</sup>Digestive and General Surgery and <sup>12</sup>Molecular and Diagnostic Pathology, Niigata University Graduate School of Medical and Dental Sciences, Niigata; <sup>13</sup>Division of Human Health and Medical Science, Graduate School of Kuroshio Science, Kochi University, Nankoku; and <sup>14</sup>Division of Novel Therapy for Cancer, The Advanced Clinical Research Center, The Institute of Medical Science, The University of Tokyo, Tokyo, Japan

**Note:** Supplementary data for this article are available at Cancer Research Online (<http://cancerres.aacrjournals.org/>).

T. Niinuma and H. Suzuki contributed equally to this work.

**Corresponding Authors:** Hiromu Suzuki, Department of Molecular Biology, Sapporo Medical University; S1, W17, Chuo-Ku, Sapporo 060-8556, Japan. Phone: 81-11-611-2111; Fax: 81-11-622-1918; E-mail: [hsuzuki@sapmed.ac.jp](mailto:hsuzuki@sapmed.ac.jp); and Yasuhisa Shinomura, First Department of Internal Medicine, Sapporo Medical University; S1, W16, Chuo-Ku, Sapporo 060-8543, Japan. Fax: 81-11-611-2282; E-mail: [shinomura@sapmed.ac.jp](mailto:shinomura@sapmed.ac.jp)

doi: 10.1158/0008-5472.CAN-11-1803

©2012 American Association for Cancer Research.



In addition, we recently showed that hypomethylation of repetitive DNA elements is predominantly observed in malignant GISTs, and that global hypomethylation correlates with increased chromosomal aberration (6).

miRNAs are a class of small noncoding RNAs that regulate gene expression by inducing translational inhibition or direct degradation of target mRNAs through base pairing to partially complementary sites (7). miRNAs are highly conserved among species and play critical roles in a variety of biologic processes, including development, differentiation, cell proliferation, and apoptosis. Consistent with their role in these processes, a number of studies have shown widespread alteration of miRNA expression patterns in cancer (8, 9). It has also been shown that in cancer global miRNA expression profiles, as well as expression of specific miRNAs, correlate with disease prognosis and clinical outcome (10). To date, however, only a few groups have studied miRNA expression in GISTs (11, 12), and no specific miRNAs that could serve as prognostic markers have yet been identified.

In this study, we investigated the global pattern of miRNA expression in GISTs. Our aim was to evaluate the contribution made by miRNAs to the malignant potential of GISTs and to identify predictive biomarkers. We determined that upregulation of miR-196a is strongly associated with high risk and poor prognosis in GIST patients. Furthermore, we provide evidence that overexpression of miR-196a is accompanied by upregulation of *HOXC* cluster genes and a metastasis-associated noncoding RNA in GISTs.

## Materials and Methods

### Tumor samples

A total of 56 fresh frozen GIST specimens were obtained from Sapporo Medical University Hospital, Keiyukai Sapporo Hospital, and Osaka University Hospital, as described (6). In addition, formalin-fixed paraffin-embedded (FFPE) tissue sections of 100 GIST specimens were obtained from Niigata University Hospital. Informed consent was obtained from all patients before collection of the specimens, and this study was approved by the respective Institutional Review Boards. Risk grade was assessed according to the risk definition system proposed by Fletcher and colleagues (4). Tumors that were less than 2 cm in diameter with a mitotic count of less than 5/50 high-power fields (HPF) were categorized as very low risk. Tumors that were 2 to 5 cm in diameter with a mitotic count of less than 5/50 HPF were considered to be low risk. Tumors that were less than 5 cm in diameter with a mitotic count of 6 to 10/50 HPF, or were 5 to 10 cm with a mitotic count of less than 5/50 HPF were considered to be intermediate risk. Tumors that were more than 5 cm in diameter with a mitotic count of more than 5/50 HPF, more than 10 cm in diameter with any mitotic count, or any size with a mitotic count of more than 10/50 HPF were considered to be high risk. Total RNA was extracted from fresh frozen tissue specimens using a mirVana miRNA Isolation Kit (Ambion). Total RNA was extracted from FFPE tissue specimens using a RecoverAll Total Nucleic Acid Isolation Kit for FFPE (Ambion). Tumor tissues were reviewed by

pathologists and were macrodissected; laser capture microdissection was not carried out in this study.

### miRNA microarray analysis

One-color microarray-based miRNA expression analysis was carried out according to the manufacturer's instructions (Agilent Technologies). Briefly, 100 ng of total RNA from fresh frozen GIST tissues was labeled using miRNA Labeling Reagent (Agilent Technologies), after which the labeled RNA was hybridized to a Human miRNA Microarray V3 (Rel 12.0, G4470C; Agilent Technologies), which covers 859 human miRNAs and 80 viral miRNAs. The microarray data were analyzed using GeneSpring GX version 11 (Agilent Technologies). The normalized microarray data were then compared with the TaqMan assay results using GraphPad PRISM version 5 (GraphPad Software Inc.). The Gene Expression Omnibus accession number for the miRNA microarray data is GSE31741.

### Quantitative RT-PCR of miRNA

miR-196a expression was analyzed using TaqMan microRNA Assays (Applied Biosystems). Briefly, 5 ng of total RNA were reverse transcribed using specific stem-loop RT primers, after which they were amplified and detected using PCR with specific primers and TaqMan probes. The PCR was run in triplicate using a 7500 Fast Real-Time PCR System (Applied Biosystems), and SDS v1.4 software (Applied Biosystems) was used for comparative  $\Delta C_t$  analysis. U6 snRNA (RNU6B; Applied Biosystems) served as an endogenous control.

### Gene expression microarray analysis

One-color microarray-based gene expression analysis was carried out according to the manufacturer's instructions (Agilent Technologies). Briefly, 700 ng of total RNA were amplified and labeled using a Quick Amp Labeling Kit One-Color (Agilent Technologies), after which the synthesized cRNA was hybridized to the Whole Human Genome Oligo DNA microarray, which includes 41,000 probe sets covering 19,416 genes (G4112F; Agilent Technologies). The microarray data were analyzed using GeneSpring GX version 11 (Agilent Technologies). The Gene Expression Omnibus accession numbers for the microarray data are GSE31802 and GSE32064.

### Quantitative RT-PCR of HOTAIR

Single-stranded cDNA was prepared using SuperScript III reverse transcriptase (Invitrogen). Quantitative reverse transcriptase PCR (RT-PCR) of *HOTAIR* was carried out using a TaqMan Gene Expression Assay (Assay ID, Hs03296631\_m1; Applied Biosystems) and a 7500 Fast Real-Time PCR System (Applied Biosystems). *GAPDH* (Assay ID, Hs99999905\_m1; Applied Biosystems) served as an endogenous control.

### DNA copy number and chromatin signature analysis

DNA copy number was analyzed using array-based comparative genome hybridization (CGH) as described previously (6). Trimethylated Histone H3 lysine 4 (H3K4me3) was analyzed using chromatin immunoprecipitation (ChIP) as described previously (13, 14). Details of the experimental procedures are provided in the Supplementary Methods.



### Transfection of miRNA inhibitors and siRNA molecules

GIST-T1 cells were described previously (15). For inhibition of miR-196a, cells ( $3 \times 10^5$  cells in 6-well plates) were transfected with 100 pmol of Anti-miR miRNA Inhibitors (Ambion) or Anti-miR miRNA Inhibitors Negative Control #1 (Ambion) using Lipofectamine2000 (Invitrogen). For RNA interference (RNAi)-mediated knockdown of *HOTAIR*, 3 different Stealth siRNAs against *HOTAIR* were generated by Invitrogen, after which a mixture of the 3 was used for transfection. Cells ( $3 \times 10^5$  cells in 6-well plates) were transfected with 100 pmol of siRNA or with Stealth RNAi Negative Control Medium GC (Invitrogen) using Lipofectamine2000 (Invitrogen). Total RNA extraction, cell viability assays, and Matrigel invasion assays were carried out 48 hours after transfection as described in the Supplementary Methods.

### Statistical analysis

All gene expression levels were log transformed for subsequent statistical analysis because the distribution of expression data seemed to follow a log-normal distribution. Geometric means were therefore calculated as summary statistics for expression levels. Comparisons of continuous variables were made using *t* tests or one-way ANOVA with post hoc multiple comparisons (Games–Howell test). Pearson's correlation coefficients were calculated to describe the strength of the correlation between 2 variables. Comparisons of categorical variables were made using Fisher exact test. To assess the association between prognostic factors and gene expression levels, logistic or Cox regression analyses were carried out. For these regression analyses, the most optimal cutoff points were employed to calculate ORs and HRs, with or without adjustment for clinical factors. Kaplan–Meier curves were plotted to compare 2 groups stratified by gene expression status. All statistical analyses were done using SPSS Statistics 18 (IBM Corporation).

## Results

### Detection of upregulated miR-196a expression in high-risk GISTs

To examine the miRNA expression signature in GISTs, we carried out miRNA microarray analysis with 32 fresh frozen GIST specimens (10 low-risk, 8 intermediate-risk, and 14 high-risk GISTs). The clinicopathologic features of the 32 patients are listed in Supplementary Table S1. Of 939 probe sets, 470 were excluded because of the absence of a detectable signal in any of the samples tested. Unsupervised hierarchical clustering using the remaining 469 probe sets revealed that GISTs in which there was abundant expression of miRNAs encoded on chromosome 14q32.31 form a separate cluster (Supplementary Figs. S1 and S2). Moreover, by comparing the miRNA expression profiles with array CGH results, we found that this cluster is enriched in tumors without 14q loss. These results are consistent with recent reports showing an inverse relationship between 14q loss and expression of miRNAs located on 14q in GISTs (11, 12), which is indicative of the reliability of our microarray analysis. We next carried out a scatter plot analysis and found that miR-196a is markedly upregulated in high-risk

GISTs, as compared with low- or intermediate-risk GISTs (Fig. 1A). As shown in Fig. 1B, miR-196a was undetectable in all but one of the low- and intermediate-risk GISTs tested, whereas it was upregulated in more than half of the high-risk tumors. The elevated expression of miR-196a was observed in both gastric and small intestinal GISTs (Supplementary Table S1).

### Upregulation of miR-196a is associated with GIST malignancy

To assess the clinical importance of miR-196a upregulation in GISTs, we next carried out TaqMan assay with 56 fresh frozen GIST specimens (discovery cohort), including the 32 specimens initially analyzed by microarray. The clinicopathologic features of the patients are summarized in Table 1. The TaqMan assay results were highly consistent with the microarray data, though the TaqMan assay did reveal low levels of miR-196a expression in samples in which there was no detectable signal from the microarray (Supplementary Fig. S3).

Also consistent with the microarray results was the finding that miR-196a was markedly upregulated in high-risk GISTs, as compared with the other groups ( $P = 0.004$ , one-way ANOVA; Fig. 1C, Supplementary Table S2). In addition, logistic regression analysis revealed that the association between miR-196a upregulation and the high-risk category was highest when we employed a cutoff value of miR-196a/U6 0.4 or more (OR = 13.7; 95% CI: 3.4–54.6;  $P < 0.001$ ; Supplementary Table S3). Survival data were obtained for 32 patients, and Cox hazard analysis revealed the highest HR for patients with elevated miR-196a expression when a cutoff value of 1.4 was employed (Table 2). Kaplan–Meier analysis showed poor overall survival among patients with GISTs expressing high levels of miR-196a, though the effect was not statistically significant (Fig. 1D).

We next used TaqMan assay to analyze an independent validation cohort consisting of 100 FFPE GIST specimens (Table 1). Consistent with the findings summarized above, we observed that upregulation of miR-196a was associated with high-risk GISTs (Fig. 1C, Supplementary Tables S2 and S3). By using the same cutoff value (miR-196a/U6  $\geq 1.4$ ), Cox hazard analysis revealed an elevated HR for patients exhibiting high levels of miR-196a expression (Table 2), and Kaplan–Meier analysis showed shorter survival times for the same patients (Fig. 1D). These results confirmed the prognostic value of miR-196a expression in both fresh frozen and FFPE GIST specimens.

Finally, we combined the GIST samples in the discovery and validation cohorts to examine the clinicopathologic significance of miR-196a. Expression of miR-196a correlated positively with high-risk grade (Fig. 1C, Supplementary Tables S2 and S3), poor clinical outcome (Fig. 1D, Table 2), tumor size, mitotic count, and metastasis (Table 3). Interestingly, although expression of miR-196a was not associated with age or gender, it was strongly associated with tumor location (Table 3). The median level of miR-196a expression was lowest in specimens from esophageal GISTs and then increased as the GIST site moved from the oral side toward the anal side of the gastrointestinal tract ( $P < 0.001$ ; Table 3, Supplementary Fig. S4). Importantly, although the average level of miR-196a expression was higher in small intestine than in stomach, it was positively



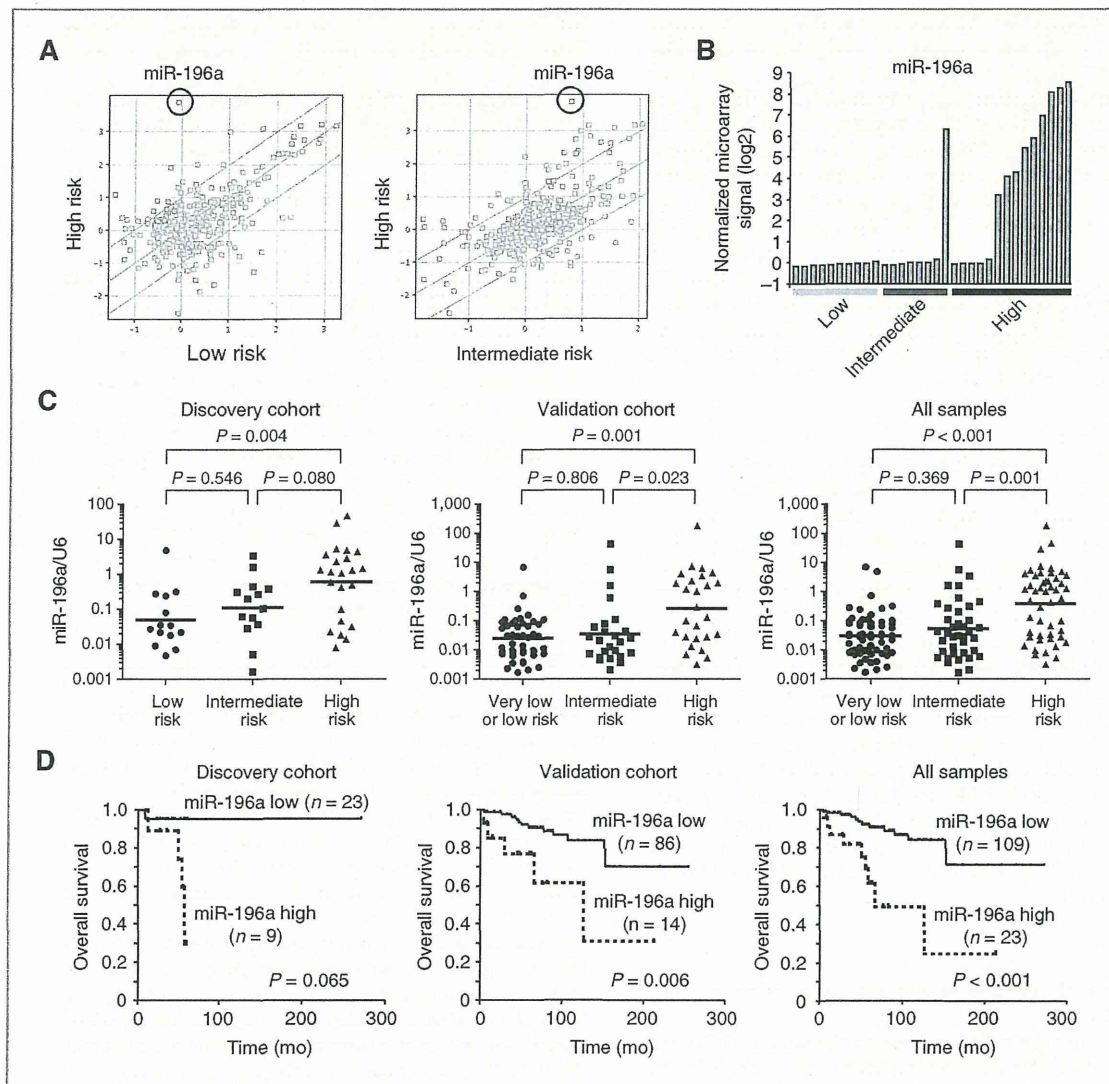


Figure 1. Upregulation of miR-196a expression in GISTs is associated with a high-risk grade and poor prognosis. **A**, scatter plots analyses: plotting low-risk ( $n = 10$ ) versus high-risk GISTs ( $n = 14$ ; left) and intermediate-risk ( $n = 8$ ) versus high-risk GISTs ( $n = 14$ ; right) revealed overexpression of miR-196a in high-risk GISTs. Microarray data are normalized and log transformed (base 2). Expression of miR-196a is highlighted by a circle. **B**, levels of miR-196a expression obtained from microarray analysis of 32 GIST specimens. Risk categories are indicated below. **C**, comparison of miR-196a expression using TaqMan assay in low- ( $n = 14$ ), intermediate- ( $n = 14$ ), and high-risk GISTs ( $n = 23$ ) in a discovery cohort (left), very low- or low-risk ( $n = 46$ ), intermediate-risk ( $n = 25$ ), and high-risk GISTs ( $n = 26$ ) in a validation cohort (middle) and all GIST specimens (right). Results are normalized to internal U6 snRNA. **D**, Kaplan-Meier curves showing the effect of miR-196a expression (high, miR-196a/U6  $\geq 1.4$ ; low, miR-196a/U6  $< 1.4$ ) on overall survival in the discovery cohort (left), validation cohort (middle), and all GIST patients (right).

correlated with high-risk grade in both organs (Supplementary Table S4).

#### Concurrent upregulation of miR-196a and HOX cluster genes in GISTs

To analyze the relationship between miR-196a upregulation and the global gene expression profiles in GISTs, we selected

age-, gender-, and tumor location-matched GIST specimens showing either low ( $n = 7$ ; average miR-196a/U6 = 0.1) or high miR-196a expression ( $n = 7$ ; average miR-196a/U6 = 15.7) and subjected them to gene expression microarray analysis (Supplementary Table S5). We found that for 4,947 probe sets (corresponding to 3,206 unique genes), there was more than a 2-fold difference in expression between GISTs with miR-196a



**Table 1.** Clinical features of the GIST samples used in this study

Discovery cohort	
Age (y, median $\pm$ SD)	68.0 $\pm$ 15.2
Gender	
Male	32 (57.1%)
Female	24 (42.9%)
Tumor location	
Stomach	40 (71.4%)
Small intestine	14 (25.0%)
Omentum	1 (1.8%)
Colorectum	1 (1.8%)
Risk category (n = 51)	
Low	14 (27.5%)
Intermediate	14 (27.5%)
High	23 (45.0%)
Validation cohort	
Age (y, median $\pm$ SD)	64.0 $\pm$ 12.4
Gender	
Male	44 (44.0%)
Female	56 (56.0%)
Tumor location	
Esophagus	5 (5.2%)
Stomach	84 (84.0%)
Small intestine	8 (8.0%)
Colorectum	3 (3.0%)
Risk category (n = 97)	
Very low	1 (1.0%)
Low	45 (46.4%)
Intermediate	25 (25.8%)
High	26 (26.8%)

overexpression and those without it. Hierarchical clustering analysis using the 4,947 probe sets clearly distinguished between tumors on the basis of their miR-196a expression status (Fig. 2A), and Gene Ontology analysis suggested that genes related to "immune system," "plasma membrane," and "cell communication" are strongly overrepresented among the differentially expressed genes (Supplementary Table S6).

To further characterize the differentially expressed genes, we carried out a gene set analysis and obtained the highest enrichment score with the *HOX* gene set (Supplementary Table S7). We found miR-196a to be encoded at 2 paralogous loci, *miR-196a-1* and *miR-196a-2*, which are located within the *HOXB* and *HOXC* clusters, respectively (Fig. 2B; ref. 16). Hierarchical clustering analysis using the expression data for *HOXC* genes clearly differentiated the GIST samples into 2 groups, and we observed perfect correspondence between higher expression of multiple *HOXC* genes and upregulation of miR-196a (Fig. 2C). By contrast, genes in other *HOX* clusters did not show such obvious correlations with miR-196a (Fig. 2C, Supplementary Fig. S5). We next compared the microarray signal for each *HOX* gene with the miR-196a expression and found strong positive correlations between the expression levels of a number of *HOXC* genes and those of miR-196a (Fig. 3D, Supplementary Fig. S6). Notably, we also found that expression of *HOTAIR*, which encodes a large intergenic non-coding RNA (lincRNA) and is located in an antisense orientation relative to the *HOXC* genes, is concurrently upregulated with miR-196a (Fig. 2C and D). Levels of miR-196a expression also correlated moderately with those of the *HOXB* genes neighboring *miR-196a-1* (*HOXB13* and *HOXB9*), but the correlations were less significant than those with *HOXC* genes (Supplementary Fig. S7).

The similarity between the expression patterns of *HOXC* genes and those of the noncoding RNAs encoded in the same locus is indicative of a common regulatory mechanism involved in the activation of these genes in GISTs. However, array CGH analysis of 27 GIST specimens failed to detect either gain or loss in any *HOX* loci, irrespective of *miR-196a* or *HOX* gene expression, which makes it unlikely that genomic amplification is the cause of their overexpression (Supplementary Fig. S8).

#### Upregulation of *HOTAIR* is associated with GIST malignancy

A recent study showed that *HOTAIR* is overexpressed in primary breast cancer and is associated with metastasis (17). To examine its clinical significance in GISTs, we carried out TaqMan assays of *HOTAIR* with the discovery cohort samples. We found that the microarray signals for *HOTAIR* were highly

**Table 2.** miR-196a expression is associated with poor clinical outcome in GIST patients

	miR-196a/U6	Outcome					
		Survival	Death	HR (95% CI)	P	HR <sup>a</sup> (95% CI)	P
Discovery cohort	<1.4	22	1				
	$\geq$ 1.4	5	4	6.3 (0.7–57.5)	0.104	32.9 (2.0–551.3)	0.015
Validation cohort	<1.4	73	13				
	$\geq$ 1.4	9	5	3.9 (1.4–11.1)	0.011	8.4 (2.6–26.9)	<0.001
All samples	<1.4	95	14				
	$\geq$ 1.4	14	9	4.9 (2.1–11.7)	<0.001	9.1 (3.5–23.7)	<0.001

<sup>a</sup>Age and gender adjusted HR.



**Table 3.** Correlation between miR-196a expression and clinicopathologic features of GISTs

	<i>n</i>	miR-196a/U6		<i>P</i>		
		Geometric mean	95% CI			
Age (y)						
<65	76	0.093	0.051–0.168			
≥65	81	0.074	0.044–0.127	0.581		
Gender						
M	76	0.104	0.059–0.186			
F	80	0.069	0.040–0.119	0.297		
Location						
Esophagus	5	0.019	0.001–0.417	Ref		
Stomach	124	0.061	0.039–0.094	0.741	Ref	
Small intestine	22	0.395	0.163–0.957	0.161	0.002	Ref
Colorectum	4	4.936	2.564–9.502	0.023	<0.001	<0.001
				<0.001		
Tumor size (cm)						
≤5.0	70	0.045	0.026–0.075			
>5.0	81	0.118	0.066–0.210	0.016		
Mitotic count (/50 HPF)						
≤5	105	0.036	0.025–0.053			
>5	35	0.539	0.215–1.353	<0.001		
Metastasis						
Yes	28	0.747	0.307–1.819			
No	108	0.041	0.027–0.063	<0.001		

consistent with the TaqMan assay results (Supplementary Fig. S9). *HOTAIR* was upregulated exclusively in high-risk GISTs, as compared with low- or intermediate-risk GISTs ( $P = 0.018$ ; Fig. 3A), and its expression correlated positively with the expression of miR-196a (Fig. 3B) and *HOXC* genes (Fig. 3C, Supplementary Fig. S10). In addition, logistic regression analysis revealed that high levels of *HOTAIR* expression in GISTs ( $HOTAIR/GAPDH \geq 0.0002$ ) were strongly associated with metastasis (age and gender adjusted OR = 8.2; 95% CI: 1.4–48.4;  $P = 0.021$ ). Cox hazard analysis suggested an elevated HR for patients with high *HOTAIR* expression (Table 4), and Kaplan–Meier analysis showed poor overall survival for the same patients, though the effect was not statistically significant (Fig. 3D). We also tried to analyze *HOTAIR* expression in the FFPE specimens; however, we failed to detect expression of either *HOTAIR* or *GAPDH* in these samples, most likely due to an inadequate quality of the RNA.

#### Reduced expression of miR-196a and *HOTAIR* target genes in GISTs

To examine the functional role of miR-196a in GISTs, we interrogated our gene expression microarray data for miR-196a target genes computationally predicted by TargetScan. Of the 2,248 genes whose expression was reduced in GISTs overexpressing miR-196a, 95 corresponded to predicted targets (Supplementary Fig. S11, Supplementary Table S8). This gene list included *ANXA1* (Annexin A1), which is an experimentally validated miR-196a target gene (18). In addition, expression of

several *HOX* genes, including *HOXB8*, was reduced in GISTs overexpressing miR-196a, which is consistent with an earlier finding of miR-196a-directed cleavage of *HOXB8* mRNA (Supplementary Fig. S11; ref. 19).

In normal human fibroblasts, *HOTAIR* represses *HOXD* gene expression by interacting with polycomb repressive complex 2 (PRC2; ref. 20). In breast cancer cells, overexpression of *HOTAIR* was shown to recruit PRC2 to more than 800 gene promoters, leading to histone H3K27 methylation and epigenetic silencing of the target genes (17). We therefore examined our microarray data for the reported *HOTAIR*-induced PRC2 target genes. Among 14 GISTs analyzed with the microarray, all 7 tumors strongly expressing miR-196a showed elevated *HOTAIR* expression (average  $HOTAIR/GAPDH = 0.00254$ ), whereas all tumors only weakly expressing miR-196a showed little or no *HOTAIR* expression (average  $HOTAIR/GAPDH = 0.00001$ ). We found that expression of 144 *HOTAIR* target genes was reduced in GISTs overexpressing *HOTAIR* (Supplementary Fig. S11, Supplementary Table S9). These results indicated that overexpression of miR-196a and *HOTAIR* may contribute to the malignant progression of GISTs by modulating expression of their target genes.

#### Inhibition of miR-196a and *HOTAIR* suppresses GIST cell invasion

We next utilized a cultured GIST cell line to determine whether upregulation of miR-196a and *HOTAIR* is responsible for the malignant potential of GISTs. We found that both

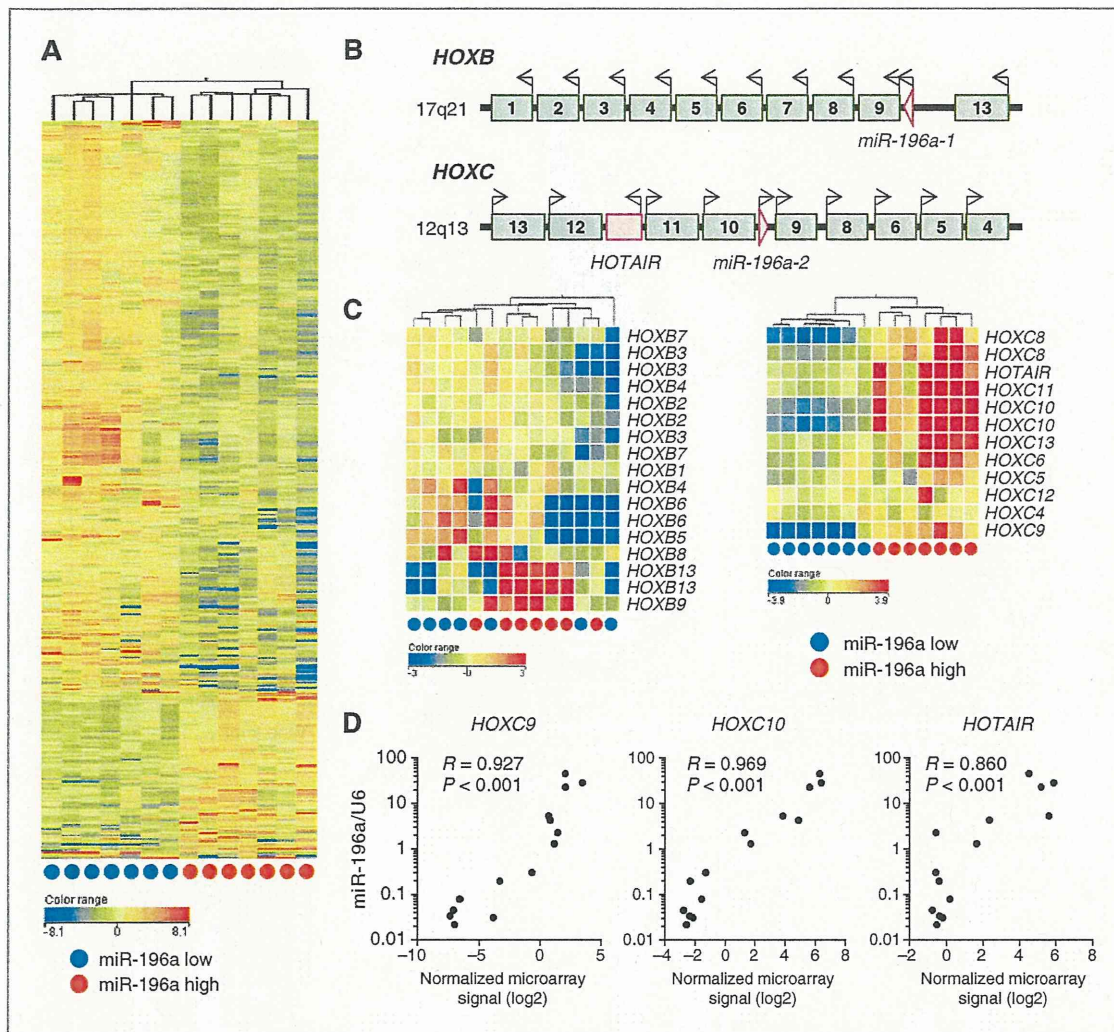


Figure 2. *GIST* gene expression signatures reveal a strong correlation between the *miR-196a* and *HOXC* genes. A, heat map of the gene expression signatures correlated with *miR-196a* expression. Rows represent probe sets and columns represent patients. A total of 4,947 probe sets differentially expressed (>2-fold change) between *GISTs* with ( $n = 7$ ) and without ( $n = 7$ ) *miR-196a* overexpression were selected, after which hierarchical clustering was carried out. The *miR-196a* expression status is indicated below. B, schematic representations of the *miR-196a* family locations within the *HOXB* and *HOXC* gene clusters. C, hierarchical clustering analysis using *HOXB* (left) and *HOXC* (right) expression data. *miR-196a* expression status is indicated below. D, correlations between the expression levels of *miR-196a* and *HOXC* genes or *HOTAIR*. Expression of *miR-196a* was analyzed using TaqMan assay and was normalized to internal U6 snRNA. Microarray data for *HOXC* and *HOTAIR* were normalized and log transformed (base 2). The Pearson correlation coefficients and *P* values are shown.

*miR-196a* and *HOTAIR* are expressed in *GIST-T1* cells (Supplementary Fig. S12). We then carried out cell viability and Matrigel invasion assays after transfecting *GIST-T1* cells with an anti-*miR-196a* inhibitor molecule. Gene expression microarray analysis revealed that a number of predicted *miR-196a* target genes, including *ANXA1* and *HOXA5*, were upregulated by inhibition of *miR-196a* (Supplementary Table S10), and although we observed no effects on cell viability, inhibition of *miR-196a* moderately suppressed cell invasion (Supplementary Fig. S13). We next disrupted *HOTAIR* expression by

transfecting the cells with siRNAs targeting it (Fig. 3E). Although knockdown of *HOTAIR* did not significantly affect cell viability, it suppressed the invasiveness of *GIST-T1* cells (Fig. 3E and F). Moreover, gene expression microarray analysis revealed that a number of reported *HOTAIR* target genes, including *PCHD10*, *SEMA6A*, and *STK17B*, were upregulated upon knockdown of *HOTAIR* (Supplementary Table S11). In all, we found that 1,424 genes were upregulated by siHOT (>2-fold), and Gene Ontology analysis revealed enrichment of genes related to "nucleus," "chromosome," and "membrane-bounded